

DEVELOPMENT AND OPTIMIZATION OF THE WOUND HEALING ELECTROSPUN POLYURETHANE/COLLAGEN/PHYTOCERAMIDES NANOFIBERS USING THE BOX-BEHNKEN EXPERIMENTAL DESIGN (QUALITY BY DESIGN)

TASSNEIM M. EWEDAH^{1*}, MOHAMED EL-NABARAWI^{2*}, MAHMOUD H. TEAIMA², SAMMAR FATHY ELHABAL³, KAMEL R. SHOUEIR^{4,5}, ABDALLAH M. HAMDY⁶, AHMED ABDALLA¹

¹Department of Pharmaceutics and Pharmaceutical Technology, Faculty of Pharmacy, Egyptian Russian University, Badr City, PO, Cairo-11829, Egypt. ²Department of Pharmaceutics and Industrial Pharmacy, Faculty of Pharmacy, Cairo University, Kasr El-Aini Street, PO, Cairo-11562, Egypt. ³Department of Pharmaceutics and Industrial Pharmacy, Faculty of Pharmacy, Modern University for Technology and Information (MTI), Mokattam, Cairo-11571, Egypt. ⁴ICPEES, Institut de Chimie et Procédé pour l'Energie, l'Environnement et la Santé, CNRS, UMR 7515, Université de Strasbourg, 25 Rue Becquerel-67087 Strasbourg Cedex 2, France. ⁵Institute of Nanoscience and Nanotechnology, Kafrelsheikh University, Kafrelsheikh-33516. ⁶Department of Pharmaceutical Analytical Chemistry, Faculty of Pharmacy, Egyptian Russian University, Badr City, PO, Cairo-11829, Egypt
*Corresponding author: Tassneim M. Ewedah; *Email: tassneimewedah@gmail.com

Received: 20 May 2024, Revised and Accepted: 03 Jul 2024

ABSTRACT

Objective: This study aimed to develop and optimize polyurethane/collagen/phytoceramides nanofibers, a wound-healing drug delivery approach, using the electrospun technique. The objective was to enhance the effectiveness of nanofibers by optimizing the preparation process.

Methods: The box-behnken design was established to optimize the electrospinning instrument performance and, consequently, the nanofiber effectiveness. Response variables were diameter, zeta potential, and diffusion coefficient, while the experimental key factors were applied voltage, flow injection rate, and rotary collector speed of the electrospinning instrument. The optimized nanofibers were examined to ensure the validity of the optimization process.

Results: The study built prediction models for each response and employed a desirability function to suggest an optimum working level of each factor that guarantees minimum diameter, maximum zeta potential, and maximum diffusion coefficient. The desirability function suggested experimental conditions of 12.9 KV for the applied voltage, 1.3 ml/h for the injection flow rate, and a speed of 920 rpm for the rotary collector speed. The optimized formula proved satisfactory physicochemical properties regarding the nanofiber's infrared spectrum and wettability characteristics. The biomedical effectiveness of the optimized nanofibers showed increased anti-inflammatory potency up to 82.8±2.6% and a high wound closure rate of about 79%. Also, the stability study showed a nonsignificant change in response over the studied points.

Conclusion: The optimized nanofiber formula achieved the desired diameter, zeta potential, and diffusion coefficient. The results proved the Box-Behnken design approach's efficacy in enhancing the nanofiber formula's effectiveness and stability.

Keywords: Nanofiber, Wound healing, Box behnken design, Optimization, Quality by design

© 2024 The Authors. Published by Innovare Academic Sciences Pvt Ltd. This is an open access article under the CC BY license (<https://creativecommons.org/licenses/by/4.0/>)
DOI: <https://dx.doi.org/10.22159/ijap.2024v16i5.51510> Journal homepage: <https://innovareacademics.in/journals/index.php/ijap>

INTRODUCTION

Inflammation, proliferation, and remodelling are all steps in the intricate biological process of wound healing. Being the biggest organ in the body, the skin is vital in this process because it acts as a natural defence mechanism against harmful substances [1, 2]. A multi-step and dynamic process is initiated at the site of a skin injury, whether acute or chronic, when the skin's integrity is compromised. Repairing wounds entails balancing inflammatory cytokines at the site of the injury and restoring tissue integrity [3].

A unique combination of polyurethane, collagen, and phytoceramides for tissue engineering purposes was prepared. Electrospun nanofibers of polyurethane, collagen, and phytoceramides improved cell adhesion and elongation adaptability. A revolutionary idea for tissue engineering is introduced by combining these three polymers. The hydrophobic character of polyurethane is responsible for wound healing since it raises surface tension and, hence, lessens the contact between cells and the scaffold. Because they cannot connect with nearby cells, stressed cells take on a spherical shape and are unable to expand themselves like fibroblasts or carry out regular growth and reproduction [4]. Collagen is leading the way in wound treatment because it meets all of these criteria: it is ubiquitous, it has low immunogenicity, and it can be bent into strong, biocompatible scaffolds.

Additionally, collagen-based materials expertly blend synthetic and natural macromolecules. Collagen is essential for providing tissues

with both mechanical strength and flexibility. Furthermore, it is a favourable surface for cellular attachment, growth, and specialization. Collagen is used as a surface coating to improve moisture preservation and facilitate cell attachment in scaffold matrices [5-14]. Ceramides are influential in facilitating cellular effects by activating cell surface receptors, promoting cell proliferation and migration, and strengthening the skin's protective barrier [15-17].

Quality by design is an approach used in various studies to ensure an ongoing supply of high-quality products. Design of Experiments (DOE) introduces data-based evidence leading to comprehension processes from the least number of experiments [18-20]. The nanofiber preparation procedure has a critical effect on the shape and morphology of the nanofiber and, consequently, its effectiveness. The preparation process includes several parameter factors that must be controlled to obtain more effective and stable nanofibers. Several works represented the effect of different factors on the response variables of the prepared nanofibers [21-27]. However, no previous work discussed the optimization process via compromising between all factors to obtain the most optimum conditions in the preparation process, thus ensuring the best effectiveness and stability.

The current work discusses the optimization of the nanofiber preparation process. The work involves establishing a Box-Behnken design to predict the optimum experimental conditions for preparing nanofibers. The prepared optimized nanofibers were examined in terms of physicochemical properties and biomedical

effectiveness. A stability study was also performed on the dosage form before and after optimization.

MATERIALS AND METHODS

Materials

The thermoplastic polyurethane (1185A), with a density of 1.12 g/cm³, is supplied by BASF Elastollan in Germany. Vita Nuova, a company based in the United Kingdom, provides support for phytoceramides (Lipowheat, 350 mg). Triton X-100 and N, N-dimethylformamide (DMF), which is anhydrous and has a purity of 99.8%, with a chemical formula of C₃H₇NO, a solubility parameter (δ) of 12.14 (cal/cm³)^{0.5}, and a dielectric constant (ϵ) of 37, were obtained from Sigma. Sodium hydrogen phosphate (Na₂HPO₄), glacial acetic acid (CH₃COOH, 99-100%), and ethylenediaminetetraacetic acid (EDTA, (HO₂CCH₂)₂NCH₂CH₂N(CH₂CO₂H)₂) were obtained from MERCK.

Extraction of collagen

Collagen was extracted from a fresh piece of tilapia fish (*Oreochromis* sp.). The tendons were dissected into small fragments following thorough cleaning. The tendon was treated using a 0.05 M aqueous solution of Na₂HPO₄ at a temperature of 5 °C for two days. Afterwards, the tendon underwent a washing procedure using Phosphate-Buffered Saline (PBS). Next, the tendon was subjected to a solution consisting of 0.5 M acetic acid, pepsin at a concentration of 1.0 g/100 g of tissue, and a 3 mmol EDTA solution. The procedure was conducted at a temperature of 5 °C for 6 d. The diluted solution underwent centrifugation at a speed of 6000 revolutions/min for 15 min. Combine a 4 M aqueous solution of NaCl with the supernatant while stirring. Following filtration, the collagen gel solution was subjected to dialysis using distilled water at a temperature of 5 °C for two weeks until it reached a pH of 7. The freeze-drying process was carried out by subjecting the samples to a temperature of -60 °C for 24 h.

Procedures

Electrospinning of polyurethane/Collagen/Phytoceramides nanofibers (Preliminary formula)

Fabrication of polyurethane/Collagen/phytoceramides nanofibers

Before use, the polyurethane granules were subjected to a drying process in a vacuum oven at a temperature of 80 °C for 1 h to remove any moisture that had been absorbed. Afterwards, a solution was created by dissolving 3.5 g of polyurethane granules with a weight concentration of 7 weight percent in 50 milliliters of DMF solvent. As a way of fully dissolving and creating a uniform solution without any solid additives, the mixture was agitated using a magnetic stirrer for 3 h at normal room temperature. The polyurethane that had been dissolved was subsequently mixed with extracted collagen at a concentration of 5 w % concerning the polyurethane. Each mixture was agitated for an additional 4 h at room temperature until a uniform dispersion was achieved, subsequently, in the production of an electrospun polyurethane/collagen/phytoceramides fibrous film, a phytoceramides quantity of 1.5 wt. % of the solution's total weight was added to the prepared polyurethane/collagen mixture. This mixture was then transferred to the electrospinning unit. The electrospinning process was carried out with parameters including a voltage of 18 KV, a flow rate of 1.7 ml/h, a rotary speed of 650 rpm, and a distance between the needle tip and the collector of 14 cm. Subsequently, after spinning 10 ml of polyurethane/collagen/ phytoceramides dispersion, the nanofibers were carefully deposited on an aluminium-coated collector. The resulting fibers were dehumidified in a vacuum desiccator and carefully stored for later analysis.

Measurements of the prepared Polyurethane/Collagen/Phytoceramides nanofibers

Response variables, namely, diameter, zeta potential, and diffusion coefficient, were determined for the prepared nanofibers.

The functionalities of nanofibers in cell adhesion, proliferation, and tissue regeneration were shown to be significantly influenced by

their diameter. Like the extracellular matrix, smaller diameters improve cellular interactions, tissue integration, and regeneration in biomedical scaffolds. The optimization of their performance for particular applications in tissue engineering, drug delivery, and wound healing still heavily depends on precisely controlling and manipulating their diameter [28]. Thus, the morphology of the nanofibrous scaffolds and the fiber diameter were analyzed via Scanning Electron Microscopy (SEM) using ImageJ (NIH Image) software 1.8.0, Maryland, USA.

Electrostatic repulsion occurs between nanofibers possessing a high zeta potential. This repulsion increases the wetting and spreading of the liquid on the fiber surface. As a result, higher zeta potential fibers typically show better liquid absorption and increased wettability [29].

The zeta potential and translational diffusion coefficient measurements of dispersions containing nanofibers were carried out using a dynamic light scattering instrument (Malvern Zetasizer Nano ZS, Worcestershire, UK) at 25 °C in duplicate. All samples were dispersed in ethanol at a concentration of 0.1% (w/v) for both measurements.

Optimization process

Box behnken design

Box Behnken Design (BBD) was established to optimize nanofibers. The Box-Behnken design was developed using Stat graphics program version 16, where levels were carefully selected (3 levels for each factor). A set of 15 nanofiber preparations was performed according to the multilevel multifactor Box-Behnken design. The chosen design consists of fifteen runs [30], with a single sample being taken for each run. The default model is quadratic with 10 coefficients. The optimal setting of the experimental factors has been determined and is displayed.

Prediction and preparation of optimized nanofiber formula

Following the same procedures as the preliminary formula, the intended responses of nanofibers were measured for the preparations fabricated according to BBD to obtain the results used in predicting the optimum nanofiber conditions using Stat Graphics program version 16.

An estimated response surface was constructed for each response variable to obtain the optimum values statistically.

The desirability function was utilized to collectively forecast the optimal values for all response variables. Subsequently, the optimal values for all factors were concluded, and the optimized nanofiber was prepared.

Verification of the optimized nanofiber formula

The optimized nanofiber was assessed by measuring different responses in the same manner to compare the results with those of the predicted response variables (predicted by design). Calculations were made to compare the actual results with the predictions.

Evaluation of the prepared nanofiber formulas

Fourier transform infrared spectroscopy (FTIR)

Fourier transform infrared spectroscopy (FTIR) IR Affinity-1SFTIR Spectrophotometer, Japan, was used to investigate the chemical composition and newly created linkages between the electrospun components. Samples are scanned at 4 mm/s at a resolution of 2 cm over a wave number region of 4000–400 cm⁻¹. The obtained Infrared (IR) data are interpreted to examine nanofiber properties [31].

Wetting properties

The precise range of hydrophilicity in the constructed scaffolds is essential for promoting cells' initial attachment and movement. The water-attracting capabilities of the scaffolds were evaluated by measuring the static contact angle. The surface contact angle of electrospun nanofiber scaffolds was determined using the drop-shape analysis system Theta Optical Potentiometer (T-200 Biolin Sci., Finland). Exactly 200 microliters of clean water were delicately

placed onto the nanofiber surface and meticulously adjusted to align with the camera's viewpoint. Five individual drops were precisely placed in specific areas on nanofibrous scaffolds measuring $1.5 \times 1.5 \text{ cm}^2$ for each sample [32].

Cell viability

The vitality of human skin fibroblast (HSF) cells, supplied by Nawah Scientific Research Center, Cairo, Egypt, was assessed by detecting the color change of 3-(4,5-dimethylthiazol-2-yl)-2,5-diphenyl-2H-tetrazolium bromide (MTT) from yellow to purple formazan. The efficiency of this conversion process relies on the optimal performance of mitochondria. The experimental methods were carried out in a sterile setting. The cells were cultured in several successive batches for 10 d. Subsequently, the cells were introduced into the wells of 96-well plastic plates at a density of 10×10^3 cells per well, using a fresh complete growth medium. The plates were placed in a 5% CO_2 incubator, which was maintained at a temperature of 37 °C for 24 h. Two sets of wells were created for the experiment. The first group served as the negative control and contained only cells. The second group comprised cells subjected to varying concentrations (2500, 1250, 625, and 312.5 ng/ml) of possible nanofiber compositions.

Following an additional incubation period of 48 h, the liquid medium was extracted from each well. Subsequently, a volume of 20 microliters of MTT salt solution at a concentration of 2.5 µg/ml was introduced into each well. Subsequently, the plate was placed in an incubator and kept at a temperature of 37 °C in an environment enriched with 5% CO_2 for an extra 4 h duration. We added 200 µl of a solution containing 10% sodium dodecyl sulfate (SDS) in 0.01M HCL to each well to stop the reaction and scatter the generated crystals. The plates were thereafter placed in a 5% CO_2 incubator and incubated overnight at a temperature of 37 °C. Positive control was employed to guarantee total cell death under the same conditions. The control utilized a cytotoxic natural material with a concentration of 100 µg/ml. The measurement was conducted at a wavelength of 595 nm, using a reference wavelength of 620 nm [33].

Antioxidant activity

When the compound 2,2-Diphenyl-1-Picrylhydrazyl (DPPH) comes into contact with a material that removes unstable molecules, it experiences a chemical reaction that reduces its oxidation state, causing its color to change from purple to yellow. This shift happens due to a decrease in the efficacy of the antioxidants present in the material. To evaluate the antioxidant characteristics of the prospective nanofiber formulations, a nanofiber sheet measuring $1 \times 1 \text{ cm}$ (100 mg) from each sample was submerged in a solution containing 10 ml of 0.1 mmol DPPH in methanol.

The specimens were then placed in a lightless incubator at a temperature of 37 °C for several periods, including 4, 8, and 12 h. The Ultraviolet-visible (UV-visible) spectrophotometer was utilized to measure the absorbance of the solutions at a wavelength of 515 nm at predetermined time intervals. The antioxidant potency was determined by applying the following equation:

$$\text{Antioxidant potency (\%)} = \frac{\text{OD without nanofiber} - \text{OD with nanofiber}}{\text{OD without nanofiber}} \times 100 \dots [34]$$

In vitro anti-inflammatory potency

The anti-inflammatory efficacy of the nanofiber compositions was assessed *in vitro* using the protein denaturation method. This method was delineated in a prior publication with a few inconsequential modifications. Diclofenac sodium, a potent nonsteroidal anti-inflammatory medication, was employed as a reference standard. A $1 \times 1 \text{ cm}$ nanofibrous mat was introduced into a reaction mixture containing 2.0 ml of phosphate-buffered saline (pH 6.4) and 2 ml of albumin produced from freshly laid eggs (1 mmol). The solution was placed in an incubator and maintained at a temperature of 37 °C for 20 min.

The denaturation process was conducted by subjecting the solution to a temperature of 60 °C in a water bath for 15 min. The absorbance was measured at a wavelength of 660 nm, with the experiment carried out at standard ambient temperature. The experiment was

duplicated three times. The equation utilized to evaluate the inhibition of protein denaturation is as follows:

$$\text{Inhibition of denaturation (\%)} = \frac{\text{OD control} - \text{OD test sample}}{\text{OD control}} \times 100 \dots [35]$$

Wound healing assay

The migration of the cells was assessed using a wound scratch assay. We cultured the HSF cell line by placing 5 $\times 10^5$ cells/well in a 6-well plate and allowing them to incubate overnight at 37 °C in an environment containing 5% CO_2 . Subsequently, the medium was extracted, and the adhering sheets of cells were gently scraped using a sterile 10 µl pipette tip, followed by rinsing with PBS. Subsequently, we introduced 3 milliliters of low serum medium with a concentration of 1% fetal bovine serum (FBS) in Dulbecco's Modified Eagle Medium (DMEM) as treatment. The cells were then subjected to drug treatment using dosages that corresponded to the IC50 values of each substance. Cell migration into the wound space was observed and recorded using an inverted microscope and optical camera (ZEISS ZEN microscope software, blue edition) at 0, 24, and 48 h after treatment. The wound closure rate was calculated [36].

Stability study

The responses were measured following the same procedures as the preliminary formula to assess the stability of the optimized nanofiber formula. This is considered a zero-point stability approach intended to be compared with the results of other months' stability study points using Analysis Of Variance (ANOVA) statistical analysis.

An accelerated stability study was implemented on the optimized and preliminary formulas before optimization. Studies on the 1 mo accelerated point, the 2 mo accelerated point, and the 3 mo accelerated point were performed and compared with the zero stability point. At every point of acceleration, each formula was exposed to stress conditions at a temperature of 40 °C and Relative Humidity (RH) % = 75. The results were determined from different response variables (three experiments for each response) for each formula at each accelerated point. The study was also implemented at ambient temperature conditions at 1 mo, 2 mo, and 3 mo points.

A stability cabinet (40 °C and an RH of 75%) was used for the accelerated study purpose, where the prepared nanofibers were placed, and a sample was withdrawn every month for examination.

A statistical comparison using a two-way ANOVA within a 95% confidence interval [37] was performed on the results obtained from the stability study. Also, a one-way ANOVA analysis was performed to ensure the stability of the optimized formula. Statistical analysis was performed using SPSS® statistical software. Results were considered significant if the significance level was below 0.05.

RESULTS

A nanofiber drug delivery approach using polyurethane, collagen, and phytoceramides was prepared with the aim of wound healing. This combination is unique and has proven highly efficacious for tissue engineering purposes. Fig. 1 shows the main parts of the electrospinning instrument that is used for the preparation of nanofibers. The instrument parameters include a high-voltage power supply, an injection pump, and a rotary collector plate (collector drum).

This study aims to optimize the experimental conditions of the nanofiber preparation process. This involves computational steps to obtain the most effective and stable nanofiber formula.

The establishment of the Box Behnken design was performed in which levels of the selected factors, namely, voltage (X1), the flow injection rate (X2), and speed of the rotary collector drum (X3), were carefully selected (3 levels for each factor).

The optimized nanofiber was examined by measuring the diameter, zeta potential, and diffusion coefficient (Y1, Y2, and Y3, respectively). This study also involves the prediction, verification, and evaluation of the optimized nanofiber.

Nanofibers of different diameters and a linked fiber shape form randomly, as seen in fig. 2. The diameters of the nanofibers were

measured by analyzing scanning electron micrographs with the ImageJ program.

Several fibers were chosen separately for each sample, and the diameters of each were recorded. The next step was determining the

average diameter, which allowed for a thorough evaluation of the nanofiber parameters.

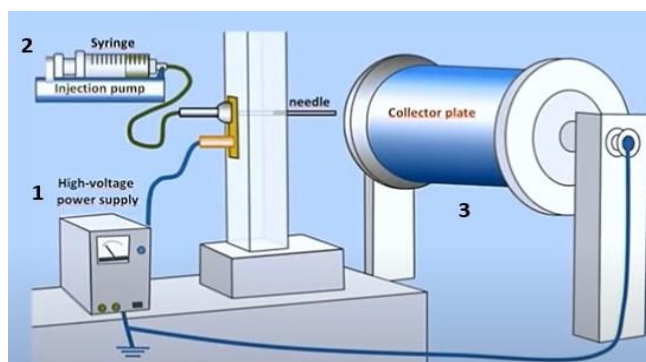


Fig. 1: Main parts of electrospinning instrument

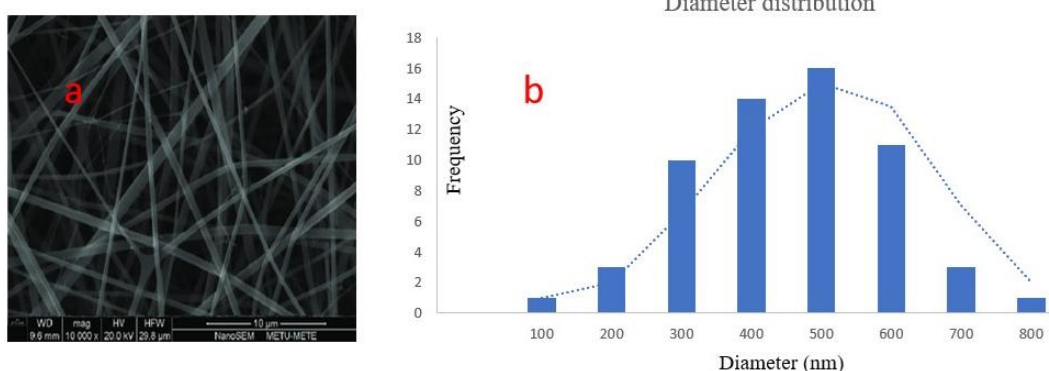


Fig. 2: SEM photograph (a) and diameter distribution of nanofibers (b)

Optimization process

Box-behnken design

Factors used in the design were voltage (X1), a flow injection rate (X2), and the speed of the rotary collector (X3). The responses, namely diameter (Y1), zeta potential (Y2), and diffusion coefficient (Y3), were observed.

For each factor, three levels were selected carefully. For the applied voltage, the three levels were 20 KV for the high level, 16 KV for the medium level, and 12 KV for the low level.

The three levels for the injection flow rate factor were 1.8 ml/h for the high level, 1.5 ml/h for the medium level, and 1.2 ml/h for the low level.

For the speed of the rotary collector factor, the three levels were 1000 rpm for the high level, 600 rpm for the medium level, and 200 rpm for the low level.

The Box-Behnken design of the fifteen prepared formulas is expressed in table 1. The intended responses were measured (three measurements for each response variable) for all the Box-Behnken-prepared nanofibers. Results are represented in table 2.

Table 1: The different conditions for formulas prepared according to the box-behnken multilevel multifactor design

Formula	Coefficient	Voltage	Flow rate	Drum collector speed
B1	Axial point (middle)	0	0	0
B2	B	-1	1	0
B3	CC (quadratic)	-1	-1	0
B4	Axial point (middle)	0	0	0
B5	AA (quadratic)	0	-1	-1
B6	B	0	1	-1
B7	C	-1	0	1
B8	AC	1	0	1
B9	A	1	-1	0
B10	C	0	-1	1
B11	BC	0	1	1
B12	AB	1	1	0
B13	A	1	0	-1
B14	Axial point (middle)	0	0	0
B15	BB (quadratic)	-1	0	-1

A is the voltage factor. B is the flow rate factor. C is the drum collector speed factor. AB, AC, and BC are the interaction terms between the factors. AA, BB, and CC are the quadratic terms of the factors. (1) High level. (0) Medium level. (-1) Low level.

Table 2: Variable response data from the fifteen formulas prepared according to the box-behnken multifactor design

Formula	Diameter (nm)	Zeta potential (\approx mV) Mean \pm SD*	Diffusion coefficient ($\mu\text{m}^2/\text{S}$)
B1	590 \pm 0.58	14 \pm 0.91	0.420 \pm 0.41
B2	572 \pm 1.02	17 \pm 0.38	0.452 \pm 0.06
B3	399 \pm 0.87	20 \pm 1.61	0.604 \pm 0.45
B4	567 \pm 0.62	13 \pm 0.47	0.441 \pm 0.08
B5	580 \pm 0.93	12 \pm 1.28	0.524 \pm 0.22
B6	812 \pm 0.58	16 \pm 0.98	0.367 \pm 0.12
B7	598 \pm 1.17	18 \pm 0.62	0.650 \pm 0.07
B8	649 \pm 1.45	15 \pm 1.18	0.295 \pm 0.34
B9	471 \pm 0.43	12 \pm 1.09	0.356 \pm 0.57
B10	517 \pm 1.05	15 \pm 1.36	0.488 \pm 0.19
B11	602 \pm 1.55	13 \pm 0.80	0.394 \pm 0.03
B12	715 \pm 1.67	11 \pm 0.72	0.341 \pm 0.29
B13	746 \pm 0.84	15 \pm 1.05	0.311 \pm 0.04
B14	585 \pm 0.07	13 \pm 1.33	0.433 \pm 0.62
B15	619 \pm 1.22	23 \pm 1.28	0.383 \pm 0.09

*Data are expressed as the mean \pm standard deviation of three experiments (n = 3).

Standard Pareto charts

To represent the effect of different factors and their interactions (in descending order of significance) on the dependent variables, standard Pareto charts were constructed for all response variables, showing the significant factors that affect each response variable.

Statistical models have been fitted to the response variables. Models with *P-values* below 0.05 indicate that the model is statistically significant at the 5.0% significance level.

The results obtained by preparations designed by Box-Behnken design were statistically analyzed using ANOVA statistical analysis within a 95% confidence interval. The significant results observed for all response variables are recorded in table 3.

The ANOVA table partitions the variability in all response variables, namely, diameter, zeta potential, and diffusion coefficient, into separate pieces for each effect. It then tests the statistical significance of each effect by comparing the mean square against an estimate of the experimental error. In this case, effects have *P-values* less than 0.05, indicating that they are significantly different from zero at the 95.0% confidence level. As shown in table 3, the

tabulated *F* values were found to be less than the calculated ones, indicating that a significant difference is present.

The values for the different response variables were analyzed, and a mathematical model for each response variable was constructed.

Effects on diameter

Effects on diameter (Y_1) were studied. The Y_1 response average ranged from 399 nm in B3 to 812 nm in B6, as shown in table 2. It was found that all factors are responsible for the difference in the diameter of the nanofiber, as displayed in the Pareto chart of Y_1 , fig. 3. Fig. 4 shows a direct relationship between both (X_1) and (X_2), and the diameter (Y_1) while showing almost an inverse relationship between (X_3) and the diameter (Y_1). At the same level of X_2 and X_3 in B3 and B9, the rise in voltage from 12 KV to 20 KV was correlated with the increase in diameter average from 399 nm to 471 nm. Also, at the same level of X_1 and X_3 in B5 and B6, the rise in the flow injection rate from 1.2 ml/h to 1.8 ml/h was correlated with the increase in diameter average from 580 nm to 812 nm. In contrast, the rise of the speed of the rotary collector from 200 rpm in B5 to 1000 rpm in B10 was correlated with the decrease in diameter average from 580 nm to 517 nm at the same level of other factors X_1 and X_2 .

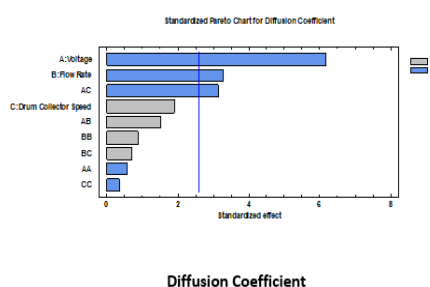
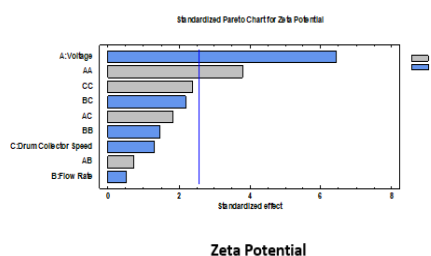
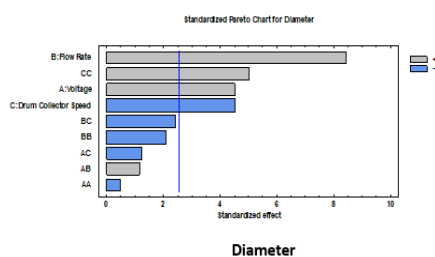


Fig. 3: A standardized pareto chart of all response variables shows significant factors that affect each response variable in formulas prepared according to the box-behnken design

Table 3: ANOVA statistical analysis within a 95% confidence interval on response variables data obtained from the fifteen preparations designed according to the box-behnken design showing factors affecting each response

Dependent variable: responses						
	Coefficient	Sum of squares	df*	mean square	F**	p-value
Diameter	Factor A: Voltage	19306.1	1	19306.1	20.46	0.0063
	Factor B: Flow Rate	67344.5	1	67344.5	71.39	0.0004
	Factor C: Drum Collector Speed	19110.1	1	19110.1	20.26	0.0064
	CC	23877.6	1	23877.6	25.31	0.0040
	Total error	4716.92	5	943.383		
Zeta Potential	Factor A: Voltage	78.125	1	78.125	41.48	0.0013
	AA	27.0833	1	27.0833	14.38	0.0127
	Total error	9.41667	5	1.88333		
Diffusion Coefficient	Factor A: Voltage	0.0772245	1	0.0772245	38.10	0.0016
	Factor B: Flow Rate	0.0218405	1	0.0218405	10.78	0.0219
	AC	0.0200223	1	0.0200223	9.88	0.0256
	Total error	0.0101347	5	0.00202693		

*Degree of freedom (n-1). **The tabulated value of F. A is the voltage factor. B is the flow rate factor. C is the drum collector speed factor. AB, AC, and BC are the interaction terms between the factors. AA, BB, and CC are the quadratic terms of the factors.

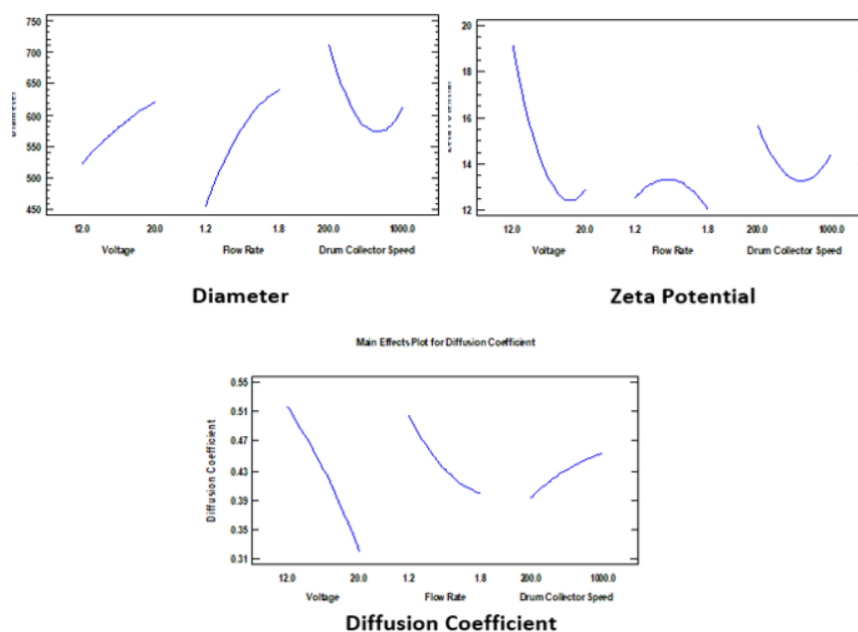


Fig. 4: The main effects of different factors on each response variable

Effects on zeta potential

Effects on zeta potential (Y_2) were investigated. The Y_2 response average ranged from 11 mV in B12 to 23 mV in B15, as shown in table 2. It was found that the factor that is mainly responsible for the difference in the zeta potential of the nanofiber is the applied voltage, as displayed in the Pareto chart of Y_2 , fig. 3. Fig. 4 shows almost an inverse relationship between both (X_1), and zeta potential (Y_2). At the same level of X_2 and X_3 in B3 and B9, the rise in the voltage from 12 KV to 20 KV was correlated with the lowering in the zeta potential average from 20 mV to 12 mV.

Effects on the diffusion coefficient

Effects on the diffusion coefficient (Y_3) were studied. The Y_3 response average ranged from 0.295 $\mu\text{m}^2/\text{s}$ in B8 to 0.650 $\mu\text{m}^2/\text{s}$ in B7, as shown in table 2. It was found that the applied voltage and injection flow rate factors are responsible for the difference in the diffusion coefficient of the nanofiber, as displayed in the Pareto chart of Y_3 , fig. 3. Fig. 4 shows almost an inverse relationship between both (X_1) and (X_2), and the diffusion coefficient (Y_3). At the same level of X_2 and X_3 in B3 and B9, the rise in the voltage from 12 KV to

20 KV was correlated with the decrease in diffusion coefficient average from 0.604 $\mu\text{m}^2/\text{s}$ to 0.356 $\mu\text{m}^2/\text{s}$. Also, at the same level of X_1 and X_3 in B5 and B6, the rise in the flow injection rate from 1.2 ml/h to 1.8 ml/h correlated with the decrease in diffusion coefficient average from 0.524 $\mu\text{m}^2/\text{s}$ to 0.367 $\mu\text{m}^2/\text{s}$.

Prediction and fabrication of the optimized nanofiber formula

Estimated response surface

Estimated response surfaces (fig. 5) were constructed. They showed the optimum values of the three influential factors included in the formulation process of the nanofibers, which can minimize the diameter and maximize both the nanofiber's zeta potential and diffusion coefficient. It was found that for the minimum diameter, the optimum values are 12.3 KV for the applied voltage, 1.2 ml/h for the injection flow rate, and 583.029 rpm for the speed of the rotary collector, while for the maximum zeta potential, it is 13.17 KV for the applied voltage, 1.60784 ml/h for the injection flow rate, and 200 rpm for the speed of the rotary collector. For maximum diffusion coefficient, these are the values of 12.0149 KV for voltage, 1.22 ml/h

for the injection flow rate, and 980 rpm for the speed of the rotary collector that gives the maximum response.

Multiple response optimization was developed to obtain optimized nanofiber experimental conditions that satisfy the intended purpose. From the desirability study and multiple response optimization, it was concluded that the optimum conditions values that can compromise all

factors to produce the optimum nanofiber formula via minimizing diameter and maximizing both zeta potential and diffusion coefficient of nanofibers were found to be 12.9 KV for voltage, 1.3 ml/h for a flow rate, and 920 rpm for the speed of the rotary collector (fig. 5).

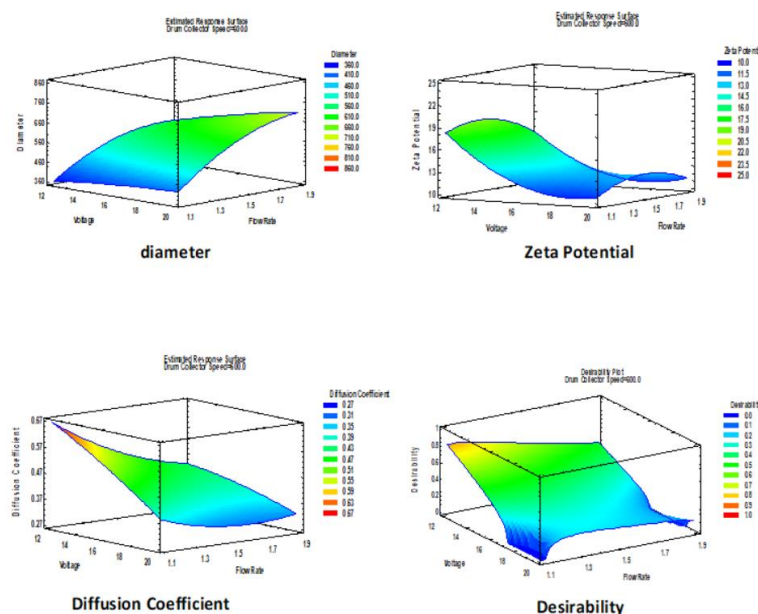


Fig. 5: The estimated response surface shows the optimum values of all factors for each response variable, and desirability shows the composition of the optimized prepared formula

Verification of the optimized nanofiber formula

All actual responses of the optimum prepared nanofiber were measured (three measurements for each response variable) and evaluated against the predicted responses using the equations:

$$\text{Prediction error (\%)} = \frac{(\text{observed value} - \text{predicted value})}{\text{predicted value}} \times 100.$$

$$\text{Residual} = \text{predicted value} - \text{observed value}$$

The expected responses of the optimized nanofiber were 503.417 nm, 20.2083 mV, and 0.699958 $\mu\text{m}^2/\text{s}$ for diameter, zeta potential, and diffusion coefficient, respectively.

The observed responses of the optimized nanofiber were found to be 511 ± 0.66 nm, 20.701 ± 0.20 mV, and 0.72 ± 0.03 $\mu\text{m}^2/\text{s}$ for diameter, zeta potential, and diffusion coefficient, respectively.

The optimized formula's residual values (difference between predicted and observed values) were 7.583 for diameter, 0.4927 for zeta potential, and 0.020042 for the diffusion coefficient (table 4).

Evaluation of the prepared nanofiber formulas

FTIR spectra

As shown in fig. 6, The nanofibrous scaffolds of both preliminary and optimized formulas exhibit distinct peaks in their FTIR spectra. The polyurethane nanofiber had identical characteristics in all scaffolds, including a carbonyl peak at 1705 cm^{-1} , C-C absorption at 1533 cm^{-1} , C-O stretching at 1112 cm^{-1} , and CH-stretching vibrations at 779 cm^{-1} , indicating the presence of substituted benzene molecules [38]. The heightened peaks validate the successful amalgamation of collagen and phytoceramides. In the polyurethane-collagen spectrum, N-H and C-H stretching peaks at 3310 cm^{-1} and 3062 cm^{-1} for amide A and

amide B indicated the presence of amino functional groups and hydrogen bonding inside the protein's N-H group. The C=O stretching was observed at a wavenumber of 1630 cm^{-1} , while the amide band II, associated with the C-N vibration, was detected at 1533 cm^{-1} [39]. The addition of phytoceramide caused the spectrum area between 3100 cm^{-1} and 2800 cm^{-1} to show two strong bands at around 2943 cm^{-1} and 2865 cm^{-1} , indicating the stretching vibrations of methylene ($\text{n}(\text{CH}_2)$). The frequency of these bands is associated with alterations in molecular structure. The polyurethane/collagen/phytoceramides nanofibers peaked around 1600 cm^{-1} , corresponding to the amide I vibration of the carbonyl group (ν C=O). Another peak around 1533 cm^{-1} is attributed to the amide II mode involving the in-plane bending of the N-H bond (δ (N-H)) and the stretching of the C-N bond (ν C-N) [40]. It appears that the amide C=O group forms strong hydrogen bonds with the amide I band due to its placement. All of these findings point to phytoceramides being integrated and held on by the scaffolds.

Wetting properties

A scaffold's wettability is an essential bio-functional feature since it facilitates the adsorption of biomolecules and proteins onto the surface of biomaterials. Protein adsorption calls for a well-balanced degree of hydrophilicity for adequate cell adhesion and colonization. Notably, cell adhesion, proliferation, and migration are all affected by the hydrophilicity of scaffolds. Adding phytoceramide lowers the water contact angle for polyurethane and collagen nanofibers [41].

The water contact angle (WCA) is a measure of wettability. Adding phytoceramides to the polyurethane/collagen mixture decreases the water contact angle and wettability. The water contact angles were found to be 58.3 ± 4.16 and 56.7 ± 3.58 for the preliminary and optimized nanofiber formulas, respectively.

Table 4: Predicted, observed values, the residuals, and the prediction error percentage for the optimized nanofiber

Response variables	Predicted*	Observed** (Experimental)	Residual ***	Prediction error (%) ****
Diameter (nm)	503.417	511 ± 0.66	7.583	1.506306

Zeta Potential (mV)	20.2083	20.701±0.20	0.4927	2.438107
Diffusion Coefficient ($\mu\text{m}^2/\text{s}$)	0.699958	0.72±0.03	0.020042	2.863315

* Value predicted by design. ** Observed data are expressed as the mean±standard deviation of three experiments (n = 3). *** Residual = predicted value – mean of the observed values. **** Prediction error (%) = (predicted value – observed values average)/predicted value × 100%.

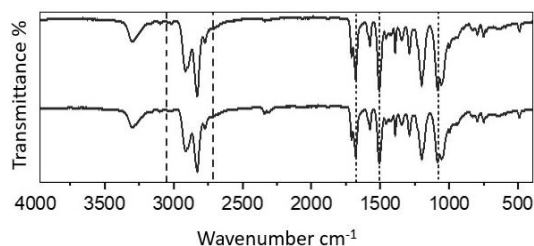


Fig. 6: FTIR spectra of preliminary and optimized formulas

Cell viability

The cytocompatibility assay was performed on the HSF cell line. The cell viability values measured for all scaffolds showed that nanofibrous scaffolds exhibited relatively high cell viability, with an estimated value of almost 100% for both optimized and preliminary nanofiber formulas at a concentration of 312.5 ng/ml. In contrast, at a higher concentration of 625 ng/ml, the cell viability dropped to 96.8±3.8% and 95.1±4.5% for the optimized and preliminary nanofiber formulas, respectively. Upon reaching the concentration of 2500, cell viability became 70.2±2.9% for the optimized nanofiber formula and 70.9±5.3% for the preliminary nanofiber formula. Based on the findings, it can be concluded that the prepared formulas are safe (non-toxic) and compatible with cells.

Antioxidant activity

During the inflammatory phase of wound healing, the skin produces a substantial quantity of reactive oxygen species (ROS) as a result of injury. This process induces cellular damage, resulting in the degradation of proteins, lipids, and nucleic acids, finally culminating in cellular demise. Consequently, the process of wound healing is interrupted. Antioxidants can greatly assist in enzymatic repair and enhance metabolism. Multiple studies have shown evidence

supporting the reliability and credibility of nanofibers as a potent source of antioxidants. This study aimed to evaluate the efficacy of nanofibrous membranes in eliminating free radicals by conducting a DPPH-free radical scavenging experiment. Both preliminary and optimized nanofiber formulas showed almost the same effectiveness in scavenging DPPH radicals at a rate of 84.5%.

In vitro anti-inflammatory potency

Wound dressing can be categorized into three distinct phases: (I) inflammation, (II) neo-tissue development, and (III) tissue remodelling [42–45]. Hence, the utilization of anti-inflammatory drugs is essential to accelerating the wound healing process. Ceramide has an impact on the different metabolic and pathophysiological pathways affected by these conditions and events in an organism. These pathways are regulated by pro-inflammatory cytokines such as TNF- α , interleukin 1 (IL-1), and IL-6 [46]. The anti-inflammatory efficacy of nanofiber formulations was evaluated in comparison to the standard diclofenac sodium treatment using a denaturation of protein assay. The standard drug showed the highest anti-inflammatory effectiveness (96.3±1.5%), followed by the optimized nanofiber formula (82.8 ±2.6%) and the preliminary nanofiber formula (80.8±2.1%).

Wound healing assay

To attain the desired level of wound closure in human skin fibroblast (HSF) cells, the nanofibrous scaffolds were put in the corresponding wells. Graphs were created at 0 h, 24 h, and 48 h to illustrate the length (measured in micrometers) of the wound area. The performance of the scaffolds was tested by examining photographs, as shown in fig. 7. After the investigation was completed, the width of the wound area was calculated using the data collected.

The results show a gradual decrease in wound width, starting from 399.6±5.8 μm and reaching 95.8±3.4 μm at 48 h, with a wound closure rate of approximately 76% for the preliminary formula. The optimized formula showed a closure rate of about 79%. The wound width decreased to 85.5±6.2 μm after 48 h.

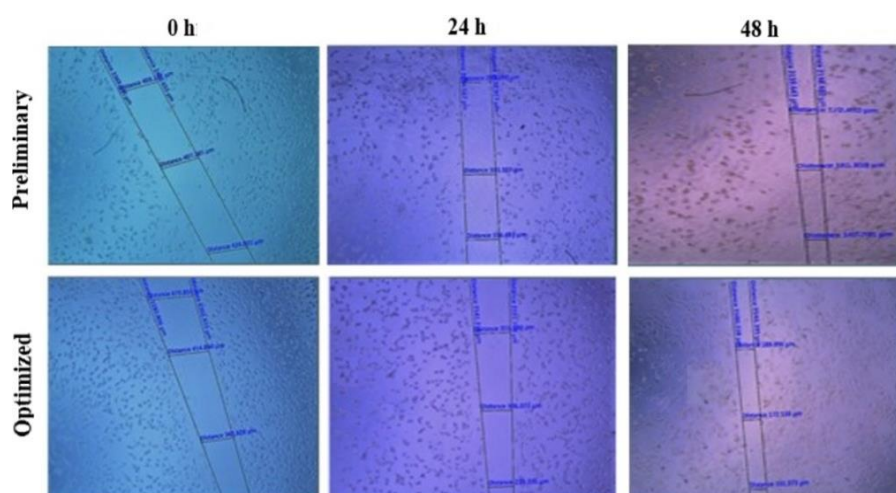


Fig. 7: The dynamic changes in wound area width over 48 h contrast the effects of preliminary and optimized nanofiber webs

Stability study

Table 5 showed that the results of the diameter and diffusion coefficient response variables obtained from stability studies performed at accelerated conditions (40 °C and 75% RH) revealed significant differences between the months' (0, 1, 2, and 3) study points. The results of the same response variables obtained from

stability studies performed at ambient temperature conditions showed no significant differences between study points (table 6).

There was no noticeable change in zeta potential findings obtained from statistical comparisons performed at different points' results at both normal ambient and accelerated conditions.

It was concluded, according to two-way ANOVA statistical analysis, that the results of the preliminary formula before optimization were significantly different from the results of the optimized one concerning diffusion coefficient at accelerated conditions (40 °C and 75% RH).

From all these findings, a separate statistical analysis (one-way ANOVA) on the results obtained from diameter and diffusion coefficient measurements for the preliminary and optimized formulas at accelerated conditions (40 °C and 75% RH) was recommended for the assessment of stability (tables 7 and 8).

Table 5: Two-way ANOVA statistical analysis within a 95% confidence interval on response variable data obtained at an accelerated stability study under 40 °C and 75% RH conditions

Two Way ANOVA		Dependent variable: responses				
Response variable*	Source	Type III sum of squares	df**	Mean square	F***	P-value
Diameter	Between Months	3872.333	3	1290.778	15.321 (3.245****)	0.000
	Between Formulae	130.667	1	130.667	1.551 (4.494 ****)	0.231
	Error	1348.000	16	84.250		
Zeta Potential	Between Months	0.391	3	0.130	0.213 (3.245****)	0.886
	Between Formulae	0.095	1	0.095	0.155 (4.494 ****)	0.699
	Error	9.796	16	0.612		
Diffusion Coefficient	Between Months	0.050	3	0.017	29.269 (3.245****)	0.000
	Between Formulae	0.031	1	0.031	54.219 (4.494 ****)	0.000
	Error	0.009	16	0.0006		

*For each response variable, three experiments (n = 3) were performed for each formula at each study point (month). **Degree of freedom (n-1). ***The calculated value of F. ****The tabulated value of F.

Table 6: Two-way ANOVA statistical analysis within a 95% confidence interval on response variable data obtained under ambient temperature conditions

Two way ANOVA		Dependent variable: responses				
Response variable*	Source	Type III sum of squares	df**	Mean square	F***	P-value
Diameter	Between Months	125.792	3	41.931	0.363 (3.245****)	0.781
	Between Formulae	2.042	1	2.042	0.018 (4.494 ****)	0.896
	Error	1850.667	16	115.667		
Zeta Potential	Between Months	0.077	3	0.026	0.050 (3.245****)	0.985
	Between Formulae	1.279	1	1.279	2.505 (4.494 ****)	0.133
	Error	8.167	16	0.510		
Diffusion Coefficient	Between Months	0.0012	3	.000405	0.590 (3.245****)	0.630
	Between Formulae	1.204E-5	1	1.204E-5	0.018 (4.494 ****)	0.896
	Error	0.011	16	0.000687		

*For each response variable, three experiments (n = 3) were performed for each formula at each study point (month). **Degree of freedom (n-1). ***The calculated value of F. ****The tabulated value of F.

Table 7: One-way ANOVA statistical analysis within a 95% confidence interval on response variable data obtained from the preliminary formula at an accelerated stability study under 40 °C and 75% RH conditions

One way ANOVA		Dependent variable: responses				
Response variable*	Source	Sum of squares	df**	Mean square	F***	P-value
Diameter	Between Groups ****	3708.667	3	1236.222	13.222 (4.07****)	0.002
	Within Groups	748.000	8	93.500		
	Total	4456.667	11			
Diffusion Coefficient	Between Groups****	0.064	3	0.021	27.574 (4.07****)	0.000
	Within Groups	0.006	8	0.001		
	Total	0.070	11			

*For each response variable, three experiments (n = 3) were performed at each study point (month). **Degree of freedom (n-1). ***The calculated value of F. ****Between study points (months). *****The tabulated value of F.

Table 8: One-way ANOVA statistical analysis within a 95% confidence interval on response variable data obtained from the optimized formula at an accelerated stability study under 40 °C and 75% RH conditions

One way ANOVA		Dependent variable: responses				
Response variable*	Source	Sum of squares	df**	Mean square	F***	P-value
Diameter	Between Groups ****	786.000	3	262.000	3.493 (4.07****)	0.070
	Within Groups	600.000	8	75.000		
	Total	1386.000	11			
Diffusion Coefficient	Between Groups ****	0.004	3	0.001	3.770 (4.07****)	0.059
	Within Groups	0.003	8	0.000		
	Total	0.007	11			

*For each response variable, three experiments (n = 3) were performed at each study point (month). **Degree of freedom (n-1). ***The calculated value of F. ****Between study points (months). *****The tabulated value of F.

DISCUSSION

The current work aims to develop and optimize a wound-healing nanofiber formula using Box-Behnken statistical design. A combination of polyurethane/collagen/phytoceramides is employed for tissue engineering using the electrospun technique, which includes many instrumental factors affecting the performance of the prepared nanofiber formulas. Electrospun parameters must be controlled to ensure the effectiveness of the synthesized nanofibers.

The factors involved in the establishment of the box-behnken design were carefully selected concerning prior reports [27, 29]. The speed of the rotary collector affects the surface area of the nanofiber and thus alters the values of both the diameter and diffusion coefficient [26]. Also, previous studies show the effect of the applied voltage of the electrospun instrument on zeta potential, diameter, and diffusion coefficient [23–25]. The flow rate of the injection can modify the morphology and porosity of nanofibers and hence their diameter and diffusion coefficient [21, 22].

Results in fig. 3 and table 3 show that the diameter is significantly affected by the voltage, injection flow rate, and speed of rotary collector factors. In contrast, the zeta potential is affected significantly by voltage. Finally, the voltage and flow rate significantly affect the diffusion coefficient. The results are well supported by other relevant literature.

The findings showed that higher voltage resulted in a reduction in both the zeta potential and diffusion coefficient. This inverse relationship can be attributed to the increased elongation of the fibers at higher voltages, leading to a more compact structure and reduced surface charge. Similar observations were made by Bhardwaj and Kundu [47], who reported that increased electrospinning voltage led to fibers with reduced zeta potential.

Better drug release and cellular interactions are probably made possible by the increased diffusion coefficient and zeta potential, which also likely contribute to the increased bioactivity. These findings are consistent with those of Chenxi Li *et al.* [48], who discovered that nanofibers with higher zeta potential and diffusion coefficients exhibit greater biological effectiveness.

The design of the experiment effectively identified the critical parameters affecting the nanofiber characteristics. The optimal conditions were determined to be 12.9 KV for the applied voltage, 1.3 ml/h for the injection flow rate, and 920 rpm for the speed of the rotary collector. These conditions produced nanofibers with a diameter of 511 ± 0.66 nm, a zeta potential of 20.701 ± 0.20 mV, and a diffusion coefficient of 0.72 ± 0.03 $\mu\text{m}^2/\text{s}$, with minimal deviations between predicted and observed values. Results represented in table 4 show slight differences (error) between observed and predicted design values, indicating that the corresponding design is valuable for optimizing the nanofiber and that the optimized prepared nanofiber achieves the desired diameter, zeta potential, and diffusion coefficient.

The physicochemical criteria examination regarding wetting properties shows that the water contact angle of the optimized nanofiber formula is 56.7 ± 3.58 , which is lower than that of the preliminary formula before optimization (58.3 ± 4.16), indicating that the hydrophilicity of the scaffolds was improved by the optimization process [49]. The reduced water contact angle between the optimized nanofibers and the initial formulations demonstrated the enhanced hydrophilicity of the optimized nanofibers. Because it encourages improved cell adhesion, proliferation, and migration on the nanofiber scaffolds, enhanced hydrophilicity is advantageous for wound healing application.

The FTIR spectra display distinct peaks, such as the carbonyl peak at 1705 cm^{-1} , the N-H and C-H stretching peaks at 3310 cm^{-1} and 3062 cm^{-1} , and the methylene stretching vibrations around 2943 cm^{-1} and 2865 cm^{-1} . These peaks provide evidence of the composite nanofibers' chemical integrity and compatibility. These results are consistent with earlier research by Chenghao Yu *et al.* [50], which showed that collagen and polyurethane-integrated nanofibers have comparable spectrum characteristics.

Furthermore, biomedical effectiveness studies, including both *in vitro* anti-inflammatory potency and wound healing assays, show significant improvement in results for the optimized formula compared with the preliminary suggested formula before optimization. Anti-inflammatory potency increased from $80.8 \pm 2.1\%$ in the preliminary nanofiber formula to $82.8 \pm 2.6\%$ in the optimized nanofiber formula. The optimized formula also shows a closure rate of about 79% after 48 h, while that of the preliminary formula before optimization was 76%. Results support the idea that the corresponding experimental design can improve the efficacy of the nanofiber formula for wound healing and tissue engineering purposes.

Also, stability study data represented in tables 7 and 8 indicates that only the optimized formula shows no significantly different results ($p > 0.05$) between the successive month's points for all response variables, suggesting that it is the formula that has the most stable results; consequently, the optimization process can enhance the stability of the preliminary dosage form.

All these findings suggest that the established design succeeded in the optimization process. The results demonstrate the efficacy of the Box-Behnken design approach in the enhancement of both the effectiveness and stability of the nanofiber formula.

CONCLUSION

Polyurethane–collagen–phytoceramide nanofibers proved highly efficacious in the wound healing process. The nanofiber preparation includes parameters that significantly affect the shape and morphology of the nanofiber and, consequently, its effectiveness and stability. Factors that mainly affected the response variables of the nanofibers were the applied voltage, injection flow rate, and the speed of the rotary collector. Optimization of the nanofibers via minimizing their diameter and maximizing both the zeta potential and diffusion coefficient of nanofibers was achieved. The optimum values of factors were found to be 12.9 KV for voltage (X1), 1.3 ml/h for flow rate (X2), and 920 rpm for the speed of the rotary collector (X3). The minimal differences obtained between the design predicted values and the observed values of the optimized nanofiber responses, satisfactory physicochemical characteristics, high biomedical effectiveness, and results of the stability study indicate that the corresponding design succeeded in optimizing the preparation process and that the optimized nanofiber verified the desired diameter, zeta-potential, and diffusion coefficient. Thus, the optimization process achieved the intended goal.

FUNDING

Nil

AUTHORS CONTRIBUTIONS

Tassneim M. Ewedah conducted the experiments and participated in the article's writing. Mohamed El-Nabarawi wrote the paper's outline and contributed to preparing and reviewing the article. Mahmoud H. Teaima was a research guide and participated in the review of the article. Sammar Fathy Elhabal participated in the discussion of the results and review of the article. Kamel R. Shoueir conducted the experiments and participated in the discussion of the results. Abdallah M. Hamdy participated in the design, analysis, and interpretation of the data. Ahmed Abdalla participated in the article's writing and discussion of the results.

CONFLICT OF INTERESTS

The authors have no conflicts of interest

REFERENCES

- Li R, Liu K, Huang X, Li D, Ding J, Liu B. Bioactive materials promote wound healing through modulation of cell behaviors. *Adv Sci (Weinheim, Baden-Wuerttemberg, Ger.)* 2022 Apr 1;9(10):e2105152. doi: [10.1002/advs.202105152](https://doi.org/10.1002/advs.202105152)
- Mienaltowski MJ, Gonzales NL, Beall JM, Pechanec MY. Basic structure, physiology, and biochemistry of connective tissues and extracellular matrix collagens. *Adv Exp Med Biol.* 2021;1348:5-43. doi: [10.1007/978-3-030-80614-9_2](https://doi.org/10.1007/978-3-030-80614-9_2)

3. Tottoli EM, Dorati R, Genta I, Chiesa E, Pisani S, Conti B. Skin wound healing process and new emerging technologies for skin wound care and regeneration. *Pharmaceutics*. 2020 Aug 1;12(8):1-30. doi: [10.3390/pharmaceutics12080735](https://doi.org/10.3390/pharmaceutics12080735), PMID [32764269](https://pubmed.ncbi.nlm.nih.gov/32764269/).
4. Kummala R, Soto Veliz D, Fang Z, Xu W, Abitbol T, Xu C. Human dermal fibroblast viability and adhesion on cellulose nanomaterial coatings: influence of surface characteristics. *Biomacromolecules*. 2020;21(4):1560-7. doi: [10.1021/acs.biomac.0c00107](https://doi.org/10.1021/acs.biomac.0c00107), PMID [32150393](https://pubmed.ncbi.nlm.nih.gov/32150393/).
5. Chattopadhyay S, Raines RT. Review collagen-based biomaterials for wound healing. *Biopolymers*. 2014;101(8):821-33. doi: [10.1002/bip.22486](https://doi.org/10.1002/bip.22486), PMID [24633807](https://pubmed.ncbi.nlm.nih.gov/24633807/).
6. Carlisle CR, Coulais C, Guthold M. The mechanical stress-strain properties of single electrospun collagen type I nanofibers. *Acta Biomater*. 2010 Aug 1;6(8):2997-3003. doi: [10.1016/j.actbio.2010.02.050](https://doi.org/10.1016/j.actbio.2010.02.050), PMID [20197123](https://pubmed.ncbi.nlm.nih.gov/20197123/).
7. Hernandez Rangel A, Martin Martinez ES. Collagen based electrospun materials for skin wounds treatment. *J Biomed Mater Res A*. 2021 Sep 1;109(9):1751-64. doi: [10.1002/jbm.a.37154](https://doi.org/10.1002/jbm.a.37154), PMID [33638606](https://pubmed.ncbi.nlm.nih.gov/33638606/).
8. Noorisafa F, Razmjou A, Emami N, Low ZX, Korayem AH, Kajani AA. Surface modification of polyurethane via creating a biocompatible superhydrophilic nanostructured layer: role of surface chemistry and structure. *J Exp Nanosci*. 2016 Sep 21;11(14):1087-109. doi: [10.1080/17458080.2016.1188223](https://doi.org/10.1080/17458080.2016.1188223).
9. Mathew Steiner SS, Roy S, Sen CK. Collagen in wound healing. *Bioengineering (Basel, Switzerland)*. 2021 May 1;8(5). doi: [10.3390/bioengineering8050063](https://doi.org/10.3390/bioengineering8050063), PMID [34064689](https://pubmed.ncbi.nlm.nih.gov/34064689/).
10. Gajbhiye S, Wairkar S. Collagen fabricated delivery systems for wound healing: A new roadmap. *Biomater Adv*. 2022 Nov 1;142:213152. doi: [10.1016/j.bioadv.2022.213152](https://doi.org/10.1016/j.bioadv.2022.213152), PMID [36270159](https://pubmed.ncbi.nlm.nih.gov/36270159/).
11. Sharma S, Rai VK, Narang RK, Markandeywar TS. Collagen-based formulations for wound healing: a literature review. *Life Sci*. 2022 Feb 1;290:120096. doi: [10.1016/j.lfs.2021.120096](https://doi.org/10.1016/j.lfs.2021.120096), PMID [34715138](https://pubmed.ncbi.nlm.nih.gov/34715138/).
12. Kallis PJ, Friedman AJ. Collagen powder in wound healing. *J Drugs Dermatol*. 2018 Apr 1;17(4):403-8. PMID [29601617](https://pubmed.ncbi.nlm.nih.gov/29601617/).
13. Babu PA, Sekhar AC, Vishnu. From seizures to wounds: the potential of phenytoin in traumatic wound management. *Int J Pharm Pharm Sci*. 2023;15(6):55-8. doi: [10.22159/ijpps.2023v15i6.48079](https://doi.org/10.22159/ijpps.2023v15i6.48079).
14. Reddy DV, Tejaswi C. Comparison of autologous platelet gel and conventional dressing in the healing of chronic wounds. *Int J Curr Pharm Sci*. 2023;15(5):83-7. doi: [10.22159/ijcpr.2023v15i5.3060](https://doi.org/10.22159/ijcpr.2023v15i5.3060).
15. Uchida Y, Park K. Ceramides in skin health and disease: an update. *Am J Clin Dermatol*. 2021 Nov 1;22(6):853-66. doi: [10.1007/s40257-021-00619-2](https://doi.org/10.1007/s40257-021-00619-2), PMID [34283373](https://pubmed.ncbi.nlm.nih.gov/34283373/).
16. Tessema EN, Gebre Mariam T, Schmelzer CE, Neubert RH. Isolation and structural characterization of glucosylceramides from ethiopian plants by LC/APCI-MS/MS. *J Pharm Biomed Anal*. 2017 Jul 15;141:241-9. doi: [10.1016/j.jpba.2017.04.036](https://doi.org/10.1016/j.jpba.2017.04.036), PMID [28463779](https://pubmed.ncbi.nlm.nih.gov/28463779/).
17. Berwick ML, Dudley BA, Maus K, Chalfant CE. The role of ceramide 1-phosphate in inflammation, cellular proliferation, and wound healing. *Adv Exp Med Biol*. 2019;1159:65-77. doi: [10.1007/978-3-030-21162-2_5](https://doi.org/10.1007/978-3-030-21162-2_5).
18. Surve C, Singh R, Banerjee A, Patnaik S, Shidhaye S. Formulation and qbd based optimization of methotrexate-loaded solid lipid nanoparticles for an effective anti-cancer treatment. *Int J App Pharm*. 2021;13(5):132-43. doi: [10.22159/ijap.2021v13i5.42373](https://doi.org/10.22159/ijap.2021v13i5.42373).
19. Panda R, Lankalapalli S. Design of experiments and optimization of amorphous solid dispersion of a BCS class IV anti-platelet drug through factorial design. *Int J App Pharm*. 2023;15(6):353-64. doi: [10.22159/ijap.2023v15i6.48767](https://doi.org/10.22159/ijap.2023v15i6.48767).
20. Rajora A, Chhabra G. Quality by design approach: regulatory need, current, and future perspective. *Asian J Pharm Clin Res*. 2021;14(6):29-35. doi: [10.22159/ajpcr.2021.v14i6.33733](https://doi.org/10.22159/ajpcr.2021.v14i6.33733).
21. Zargham S, Bazgir S, Tavakoli A, Rashidi AS, Damerchely R. The effect of flow rate on morphology and deposition area of electrospun nylon 6 nanofiber. *Journal of Engineered Fibers and Fabrics*. 2012;7(4):42-9. doi: [10.1177/155892501200700414](https://doi.org/10.1177/155892501200700414).
22. Jabur AR, Najim MA, Al- Rahman SA. Study the effect of flow rate on some physical properties of different polymeric solutions. *J Phys.: Conf Ser*. 2018;1003(1):1-7. doi: [10.1088/1742-6596/1003/1/012069](https://doi.org/10.1088/1742-6596/1003/1/012069).
23. Jalal NM, Jabur AR, Allami S. Effect of electro-spinning applied voltage on electro-spun EPS membranes thickness and fibers diameters. *J Phys.: Conf Ser*. 2021;1879(3). doi: [10.1088/1742-6596/1879/3/032085](https://doi.org/10.1088/1742-6596/1879/3/032085).
24. Liu Y, Dong L, Fan J, Wang R, Yu JY. Effect of applied voltage on diameter and morphology of ultrafine fibers in bubble electrospinning. *J Appl Polym Sci*. 2011 Apr 5;120(1):592-8. doi: [10.1002/app.33203](https://doi.org/10.1002/app.33203).
25. Syed Bakar SS, Foong KM, Abdul Halif N, Yahud S. Effect of solution concentration and applied voltage on electrospun polyacrylonitrile fibers. *IOP Conf Ser Mater Sci Eng*. 2019;701(1):4-11. doi: [10.1088/1757-899X/701/1/012018](https://doi.org/10.1088/1757-899X/701/1/012018).
26. Wen Jun H, Ching Theng K. Design of a rotating drum for electrospinning setup with adjustable speed. *Res Progr Mech Manuf Eng*. 2020;1(1):64-8. doi: [10.30880/rpme.2020.01.01.008](https://doi.org/10.30880/rpme.2020.01.01.008).
27. Okutan N, Terzi P, Altay F. Affecting parameters on electrospinning process and characterization of electrospun gelatin nanofibers. *Food Hydrocoll*. 2014;39:19-26. doi: [10.1016/j.foodhyd.2013.12.022](https://doi.org/10.1016/j.foodhyd.2013.12.022).
28. Gao C, Zhang L, Wang J, Jin M, Tang Q, Chen Z. Electrospun nanofibers promote wound healing: theories, techniques, and perspectives. *J Mater Chem B*. 2021 Apr 15;9(14):3106-30. doi: [10.1039/d1tb00067e](https://doi.org/10.1039/d1tb00067e), PMID [33885618](https://pubmed.ncbi.nlm.nih.gov/33885618/).
29. Vaquette C, Babak VG, Baros F, Boulanouar O, Dumas D, Fievet P. Zeta-potential and morphology of electrospun nano- and microfibers from biopolymers and their blends used as scaffolds in tissue engineering. *Mendelev Commun*. 2008;18(1):38-41. doi: [10.1016/j.mencom.2008.01.015](https://doi.org/10.1016/j.mencom.2008.01.015).
30. Naveentaj S, Muzib YI, Radha R. Design and optimization of fluconazole-loaded pharmacosome gel for enhancing transdermal permeation and treating fungal infections through box-behken design. *Int J App Pharm*. 2023;15(1):131-40. doi: [10.22159/ijap.2023v15i1.46413](https://doi.org/10.22159/ijap.2023v15i1.46413).
31. Stuart BH. *Infrared spectroscopy: fundamentals and applications*. 1st ed. Wiley; 2004. p. 224.
32. Langwald SV, Ehrmann A, Sabantina L. Measuring physical properties of electrospun nanofiber mats for different biomedical applications. *Membr*. 2023;13(5):488. doi: [10.3390/membranes13050488](https://doi.org/10.3390/membranes13050488), PMID [37233549](https://pubmed.ncbi.nlm.nih.gov/37233549/).
33. Alnuqaydan AM, Zainy FM, Almutary AG, Sadier NS, Rah B. Tamarix articulata extract offers protection against toxicity induced by beauty products in Hs27 human skin fibroblasts. *Plos One*. 2023 Nov 1;18(11):e0287071. doi: [10.1371/journal.pone.0287071](https://doi.org/10.1371/journal.pone.0287071), PMID [37972033](https://pubmed.ncbi.nlm.nih.gov/37972033/).
34. Baliyan S, Mukherjee R, Priyadarshini A, Vibhuti A, Gupta A, Pandey RP. Determination of antioxidants by DPPH radical scavenging activity and quantitative phytochemical analysis of Ficus religiosa. *Molecules*. 2022 Feb 1;27(4). doi: [10.3390/molecules27041326](https://doi.org/10.3390/molecules27041326), PMID [35209118](https://pubmed.ncbi.nlm.nih.gov/35209118/).
35. Dharmadeva S, Galgamuwa LS, Prasadine C, Kumarasinghe N. *In vitro* anti-inflammatory activity of Ficus racemosa L. bark using albumin denaturation method. *Ayu*. 2018;39(4):239-42. doi: [10.4103/ayu.AYU_27_18](https://doi.org/10.4103/ayu.AYU_27_18), PMID [31367147](https://pubmed.ncbi.nlm.nih.gov/31367147/).
36. Jabbar AA, Abdul-Aziz Ahmed K, Abdulla MA, Abdullah FO, Salehen NA, Mothana RA. Sinomenine accelerate wound healing in rats by augmentation of antioxidant, anti-inflammatory, immunohistochemical pathways. *Heliyon*. 2024 Jan 1;10(1):e23581. doi: [10.1016/j.heliyon.2023.e23581](https://doi.org/10.1016/j.heliyon.2023.e23581), PMID [38173533](https://pubmed.ncbi.nlm.nih.gov/38173533/).
37. Remington JP. *Remington: the science and practice of pharmacy*. 21st ed. Philadelphia: Lippincott, Williams and Wilkins; 2005.
38. Unnithan AR, Barakat NA, Pichiah PB, Gnanasekaran G, Nirmala R, Cha YS. Wound-dressing materials with antibacterial activity from electrospun polyurethane-dextran nanofiber mats containing ciprofloxacin HCL. *Carbohydr Polym*. 2012 Nov 6;90(4):1786-93. doi: [10.1016/j.carbpol.2012.07.071](https://doi.org/10.1016/j.carbpol.2012.07.071), PMID [22944448](https://pubmed.ncbi.nlm.nih.gov/22944448/).

39. Riaz T, Zeeshan R, Zarif F, Ilyas K, Muhammad N, Safi SZ. FTIR analysis of natural and synthetic collagen. *Appl Spectrosc Rev.* 2018 Oct 21;53(9):703-46. doi: [10.1080/05704928.2018.1426595](https://doi.org/10.1080/05704928.2018.1426595).
40. Garidel P. The thermotropic phase behaviour of phyto-ceramide 1 as investigated by ATR-FTIR and DSC. *Phys Chem Chem Phys.* 2002;4(12):2714-20. doi: [10.1039/b200618a](https://doi.org/10.1039/b200618a).
41. Douglas T, Haugen HJ. Coating of polyurethane scaffolds with collagen: comparison of coating and cross-linking techniques. *J Mater Sci Mater Med.* 2008;19(7):2713-9. doi: [10.1007/s10856-008-3393-6](https://doi.org/10.1007/s10856-008-3393-6), PMID [18283534](https://pubmed.ncbi.nlm.nih.gov/18283534/).
42. Huang C, Dong L, Zhao B, Lu Y, Huang S, Yuan Z. Anti-inflammatory hydrogel dressings and skin wound healing. *Clin Transl Med.* 2022 Nov;12(11):e1094. doi: [10.1002/ctm2.1094](https://doi.org/10.1002/ctm2.1094), PMID [36354147](https://pubmed.ncbi.nlm.nih.gov/36354147/).
43. Jin Y, Li S, Yu Q, Chen T, Liu D. Application of stem cells in regeneration medicine. *Med Comm.* 2023 Aug 1;4(4):e291. doi: [10.1002/mco2.291](https://doi.org/10.1002/mco2.291), PMID [37337579](https://pubmed.ncbi.nlm.nih.gov/37337579/).
44. Bauer SM, Goldstein LJ, Bauer RJ, Chen H, Putt M, Velazquez OC. The bone marrow-derived endothelial progenitor cell response is impaired in delayed wound healing from ischemia. *J Vasc Surg.* 2006 Jan;43(1):134-41. doi: [10.1016/j.jvs.2005.08.038](https://doi.org/10.1016/j.jvs.2005.08.038), PMID [16414400](https://pubmed.ncbi.nlm.nih.gov/16414400/).
45. Ravichandiran V, Manivannan S. Wound healing potential of transdermal patches containing bioactive fraction from the bark of *Ficus racemosa*. *Int J Pharm Pharm Sci.* 2015;7(6):326-32.
46. Kucuk S, Niven J, Caamano J, Jones SW, Camacho-Muñoz D, Nicolaou A. Unwrapping the mechanisms of ceramide and fatty acid-initiated signals leading to immune-inflammatory responses in obesity. *Int J Biochem Cell Biol.* 2021 Jun 1;135:105972. doi: [10.1016/j.biocel.2021.105972](https://doi.org/10.1016/j.biocel.2021.105972), PMID [33864951](https://pubmed.ncbi.nlm.nih.gov/33864951/).
47. Bhardwaj N, Kundu SC. Electrospinning: a fascinating fiber fabrication technique. *Biotechnol Adv.* 2010;28(3):325-47. doi: [10.1016/j.biotechadv.2010.01.004](https://doi.org/10.1016/j.biotechadv.2010.01.004), PMID [20100560](https://pubmed.ncbi.nlm.nih.gov/20100560/).
48. Li C, Ge J, Guo Q, Wang J, Wu J, Yan Z. Polyvinyl alcohol/collagen composite scaffold reinforced with biodegradable polyesters/gelatin nanofibers for adipose tissue engineering. *Int J Biol Macromol.* 2024;263(1):130237. doi: [10.1016/j.ijbiomac.2024.130237](https://doi.org/10.1016/j.ijbiomac.2024.130237), PMID [38368980](https://pubmed.ncbi.nlm.nih.gov/38368980/).
49. Yildirim Yalcin M, Tornuk F, Toker OS. Recent advances in the improvement of carboxymethyl cellulose-based edible films. *Trends Food Sci Technol.* 2022 Nov 1;129:179-93. doi: [10.1016/j.tifs.2022.09.022](https://doi.org/10.1016/j.tifs.2022.09.022).
50. Yu C, Chen R, Chen J, Wang T, Wang Y, Zhang X. Enhancing tendon-bone integration and healing with advanced multi-layer nanofiber-reinforced 3D scaffolds for acellular tendon complexes. *Mater Today Bio.* 2024;26:101099. doi: [10.1016/j.mtbio.2024.101099](https://doi.org/10.1016/j.mtbio.2024.101099), PMID [38840797](https://pubmed.ncbi.nlm.nih.gov/38840797/).